sciendo
Power Electronics and Drives
Volume 8(43), 2023 DOI: 10.2478/pead-2023-0011

Integrated Model Predictive Control of a Single-Phase Multilevel T-type Converter for a Photovoltaic Grid Connected System under Failure Conditions

Research paper

Wassim Boudja*, Kamel Barra

LGEA Laboratory, Department of Electrical Engineering, Larbi Ben M'hidi University, Oum El Bouaghi, Algeria

Received: 31 December 2022; Accepted: 16 April 2023

Abstract: The article presents two contributions: the first is an optimised control structure for photovoltaic grid connected systems (PVGCSs). The power chain is composed of two cascaded power converters, namely, a boost converter and a five-level T-type multilevel converter. Traditionally, each power converter is controlled by a separate mode control (SMC) from the other, which is computationally intensive since each converter requires its own control system, which is not practical. The suggested control, called integrated finite set model predictive control (IFS-MPC), allows controlling cascaded converters at the same time in one stage, instead of controlling them separately. Consequently, the overall implementation system is widely reduced. The second contribution of the article is a modified IFS-MPC called modified integrated finite set-model predictive control (M-IFS-MPC), which ensures the correct functioning of the grid-tied PV system under certain faults in converter components. Indeed, when one of the DC-link capacitors fails or when one of the auxiliary switches breaks down, by selecting an appropriate choice of the DC-link capacitors' voltage reference, the proposed design allows a normal operation without intervention on the power circuit.

Keywords: *FS-MPC • T-type multilevel converter integrated FS-MPC • photovoltaic grid connected system (PVGCS) • predictive incremental conductance method (P-Inc-Cond) • fault-tolerant multilevel inverter fault tolerant PV system*

1. Introduction

Multilevel power converters have the potential to be used in medium/high voltage-high power applications (high voltage direct current (HVDC) systems, flexible AC transmission systems [FACTS], medium voltage variable speed drive systems, high-voltage grid-connected system-based renewable energies; Bughneda et al., 2021; Franquelo et al., 2008), whereas two-level inverters (2L-VSI) cannot be used in such applications due to their limited voltage rating (Kouro et al., 2010). Their main role is synthesising a pseudo-sinusoidal voltage waveform from several levels produced from capacitor voltage sources. Consequently, the harmonic content of the output currents and voltages is greatly reduced, approaching zero as the number of levels increases. In addition, the dv/dt switching stresses lead to less electromagnetic interference, and the common mode voltage is also reduced, with the possibility of operating at a lower switching frequency (Rodriguez et al., 2002).

There are mainly three families of multilevel converters: (a) the neutral point clamped converter (NPC), (b) the cascaded H-bridge inverter and (c) the flying capacitor converter. The H-bridge inverter topology uses the modular structure of converters with two voltage levels to allow the transit of high power by sharing it among a number of converters, making the global converter inefficient, costly and more complicated for the control (Villanueva et al., 2009). For Photovoltaic (PV) applications, this topology has the main advantage that each module converter is

* *Email: boudja.wassim@googlemail.com*

Open Access. © 2023 Boudja and Barra, published by Sciendo. BY-NC-ND This work is licensed under the Creative Commons Attribution NonCommercial-NoDerivatives 4.0 License.

fed by a separate DC source. This characteristic gives us the possibility to connect PV panels in each H-bridge, thus achieving independent maximum power point tracking, which improves the energetic efficiency of the overall system (Acharya et al., 2019).

The flying capacitor converter topology requires a large number of bulk capacitors and suffers input imbalance voltage, which cause bad output waveforms (Huang and Corzine, 2006). In the NPC topology, the number of clamped diodes increases excessively as the voltage level increases, causing more losses in the converter (Rodriguez et al., 2010). Other multilevel converter variants have emerged recently such as hybrid multilevel converters (active neutral point clamped converter [ANPC], hybrid ANPC converter, hybrid H-bridge converter) and T-type power converter (Abu-Rub et al., 2010; Arikesh and Parvathy, 2020; Gupta et al., 2016; Ounejjar et al., 2011; Rezaei et al., 2022; Sharifzadeh and Al-Haddad, 2019; Vemuganti et al., 2021).

The T-type converter is an advanced topology possessing the advantages of low conduction losses, high efficiency, a relatively low number of switches and fault tolerance. A single-phase T-type converter is based on a full H-bridge converter connected to an auxiliary bidirectional switch combination, giving the converter a four-quadrant functioning possibility (Ceglia et al., 2006; Ouchatti et al., 2022).

In the last decade, finite set model predictive control (FS-MPC) has appeared as an attractive alternative offering a completely different and powerful approach to control power converters. FS-MPC is nowadays very mature and is well known for its brilliant performance, such as its fast dynamic response, no need for linear controllers, no need for modulators pulse width modulation (PWM) or space vector modulation (SVM), completely different modulation approach compared to PWM, extremely simple and being able to be implemented with standard microprocessors. The method is based on the fact that a finite number of possible switching states can be generated by the power converter. The system model is used to predict the behaviour of the variables for each switching state. For the selection of the appropriate switching state to be applied to the system, a cost function must be defined and evaluated for the predicted values at each sampling time. Then, the optimal switching state that minimises the quality function is selected to apply during the next sampling interval (Vazquez et al., 2017).

The general photovoltaic grid-connected system (PVGCS) scheme is composed of two stages of power converters, namely, an maximum power point tracking (MPPT) chopper converter cascaded with a two-level voltage source inverter. Each converter is controlled independently by its own control system. The first contribution proposes an optimised control of the two power converters placed in back-to-back mode, instead of controlling them separately, which avoids the use of two control circuits, and thus, the hardware implementation is considerably reduced.

During the lifetime of a PV system, the power electronics components break down 4 to 5 times more than the rest of the power conversion chain components. The repair process causes the system to stop, and the functioning is thus interrupted. This interruption becomes a real problem if the system is placed in a stand-alone zone. The solution is to simply replace the boke components. In the literature, failure in power electronics converters is a very important topic that needs more and more attention for introducing new methods and ideas to deal with these faults from a ‘diagnostic’ point of view (Riera-Guasp et al., 2015) or from a ‘reliability’ point of view (Peyghami et al., 2020; Wang, n.d.). Regarding the inverter side, there are very few studies that treat this aspect from a control point of view using the MPC method without introducing additional components or circuits.

In Azer et al. (2020), the authors present a fault-tolerant method on an NPC inverter by subdividing the power topology into sub-inverters with modified modulating signals based on PWM. The method is limited only to open-circuited switch faults. Also, in Sebaaly et al. (2021), the authors have presented a modified FS-MPC method applied to a packed E-cell inverter. The method also deals with an open-circuited switches fault only without treating the short-circuited device fault. In addition, they have not indicated if they have added additional hardware elements. Table 1 shows a brief comparison of the aforementioned works.

In this context, a second contribution is presented that proposes certain solutions for the integrated finite set-model predictive control (IFS-MPC) system operation under certain faulty conditions such as a short-circuited capacitor and open-circuited switch. In the proposed M-IFS-MPC, we treat an additional case of a short-circuit failure. Furthermore, a combined case of the two previous failures is studied when a short-circuit failure and an open-circuit fault occur, which is not treated previously. One of the major advantages of this method is that it prevents the interruption of the system operation when a sudden fault happens, not to mention that this method suites applications where the placement of the system is difficult to reach and repair, for instance, offshore renewable systems and space applications. Across the two faulty scenarios, the control system guarantees the continuity of

Fault-tolerant technique	Contribution	Complexity	Limitations	Additional hardware
Carrier-based PWM (Azer et al., 2020)	– SPWM-based control strategy – Modifying the modulation when fault occurs – Four simultaneous fault tolerance – Maintaining the capacitor voltages balanced	Division of the inverter into sub-inverter	Open-circuit fault only	No
Switching mode operation based on FS-MPC (Sebaaly et al., 2021)	– FS-MPC-based control strategy – One fault treated that is open circuit – Maintaining the capacitor voltages balanced	Possible additional hardware for fault detection – a costly solution	Open-circuit fault only	Yes
The present paper	– FS-MPC-based control strategy – Two types of faults studied short circuit and open circuit – Two simultaneous fault tolerance – Maintaining the capacitor voltages balanced	Uses hardware of normal control for detection	/	No

SPWM, sinusoidal pulse width modulation.

Table 1. Possible voltage levels of the studied T-type inverter with their corresponding switching state.

the service, thanks to the proposed control algorithm that employs voltage sensors in dc-link side (voltage balancing sensors) and load side (load voltage sensor).

The article is organised into three sections as follows: After an introduction in Section 1, Section 2 is dedicated to the healthy operation of a grid-connected PV system, while Section 3 is devoted to the faulty operation of the grid-connected PV system. In Section 2, part 1, we show the advantage of the hybrid predictive incremental conductance MPPT over the classic one. In part 2, the PV system, which includes the T-type inverter, is controlled using the proposed integrated control strategy of the FS-MPC. The simulation results are shown in part 3. In Section 3, two scenarios of faulty operations are presented under a modified IFS-MPC to detect and reject the faulty cases without adding any hardware components. The results are after that presented and commented on in the last part. Finally, a conclusion is provided.

2. Healthy Operation of the Grid-Connected PV System

2.1. Hybrid predictive incremental conductance MPPT control

Figure 1 depicts the general PVGCS scheme. Generally, it is composed of two stages of power converters, namely, a boost converter cascaded with a 2L-VSI. Each converter is controlled independently by its own control system. The boosting stage generally uses many classic tracking control methods such as perturb and observe (P&O), incremental conductance (Inc-Cond), hill climbing (HC) and many other advanced algorithms that have been addressed previously in the specialised literature, whereas the inverting stage converts the DC energy to AC energy with different control strategies, among them FS-MPC control.

Figure 2 shows the conventional configuration of a boost converter. It elevates the input voltage V_{pv} to a higher value V_{load} through a specific switching pattern of the insulated-gate bipolar transistor (IGBT).

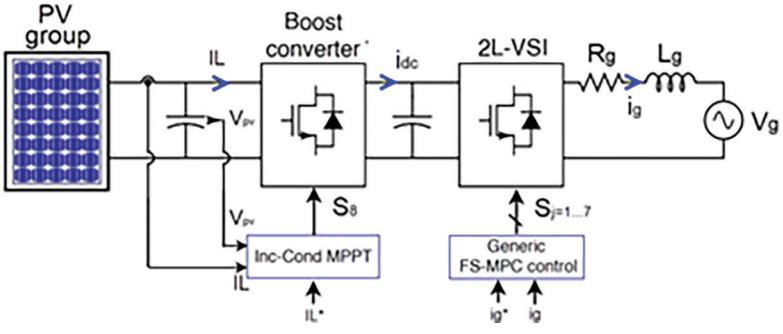

Fig. 1. General PVGCS scheme using FS-MPC control.

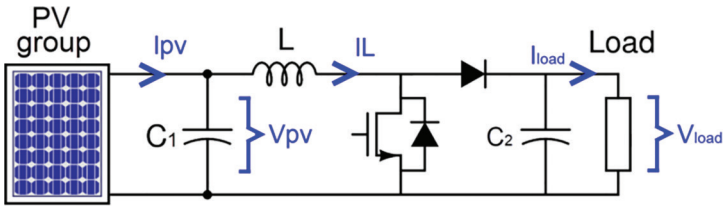

Fig. 2. Power circuit of a boost converter.

The output voltage of the boost converter is given as follows:

$$V_{load} = \frac{1}{1-D} V_{pv} \tag{1}$$

where D is the duty cycle, V_{load} is the output voltage and V_{pv} is the input PV voltage.

The boost converter contains only two states: ON and OFF and can be modelled as follows:

When the switch is turned ON (S = 1):

$$I_L(k+1) = I_L(k) + V_{pv}(k)\frac{T_s}{L} \tag{2}$$

$$V_{pv}(k+1) = V_{pv}(k) + \left(I_{pv}(k) - I_L(k)\right)\frac{T_s}{C_1} \tag{3}$$

When the switch is turned OFF (S = 0):

$$I_L(k+1) = I_L(k) + \left(V_{pv}(k) - V_{load}(k)\right)\frac{T_s}{L} \tag{4}$$

$$V_{pv}(k+1) = V_{pv}(k) + \left(I_{pv}(k) - I_L(k)\right)\frac{T_s}{C_1} \tag{5}$$

From Eqs (2)–(5), the average model of the boost converter is as follows:

$$I_L(k+1) = I_L(k) + \left(V_{pv}(k) - (1-S)\times V_{load}(k)\right)\frac{T_s}{L} \tag{6}$$

$$V_{pv}(k+1) = V_{pv}(k) + \left(I_{pv}(k) - I_L(k)\right)\frac{T_s}{C_1} \tag{7}$$

Through the specialised literature that has appeared over the last three decades (Meddour et al., n.d.; Karami, 2017), the Inc-Cond algorithm was considered the most popular MPPT control method among classical methods. Unfortunately, it continues to suffer many drawbacks, such as slow dynamic in the transient state, oscillations around maximum power point (MPP) in the steady state, possible output instability due to the use of the derivative algorithm dipv/dvpv, poor performance under shaded conditions and difficulties with the differentiation process at low levels of irradiance. To cope with these limitations, a hybrid predictive Inc-Cond control has appeared recently (Figure 3) as a powerful tool to track more closely and more efficiently the MPP for both transient and steady states.

The flowchart of the mentioned algorithm applied to a boost converter is depicted in Figure 5, where the classic Inc-Cond algorithm is used to generate the reference value of the input inductance current (Remache et al., 2019). Then, a predictive cost function g is used to minimise the current error and choose the optimal switching state of the boost converter to be applied at the next sampling time.

To well illustrate the performance of the two MPPT control methods for both transient and steady states, Figure 6 depicts the power variations under a sudden change of the illumination according to the profile [1000 – 700 – 1000]

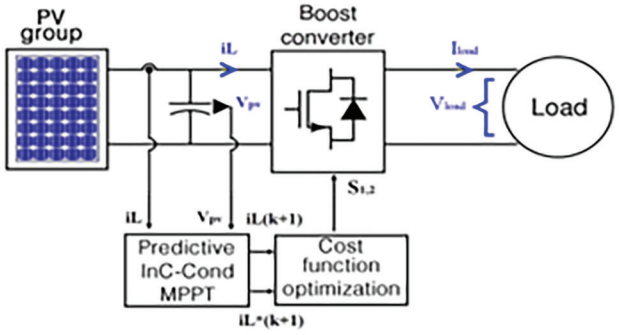

Fig. 3. Hybrid predictive Inc-Cond MPPT control scheme.

W/m^2. It is clear to see that the hybrid MPC-Inc-Cond control procures better performance than the Inc-Cond one since the MPP is tracked more accurately and more efficiently for both states.

2.2. Grid-connected PV system

2.2.1. Multilevel T-type inverter

The T-type inverter is an advanced multilevel power converter topology having several advantages over the classic 2L-VSI such as operation with voltages over the switching device rating, reduced common-mode voltages and smaller voltage changes (dv/dt). The five-level T-type inverter is composed of an H-bridge and auxiliary bidirectional controllable switches, as shown in Figure 4. This latter auxiliary structure permits the provision of more voltage

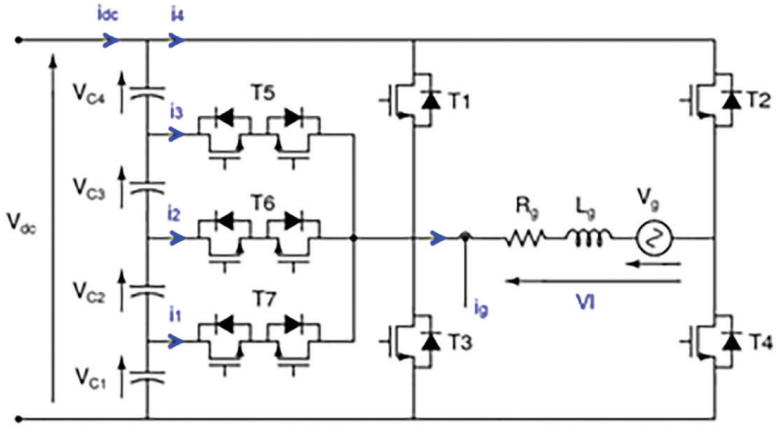

Fig. 4. Power circuit of the five-level T-type inverter.

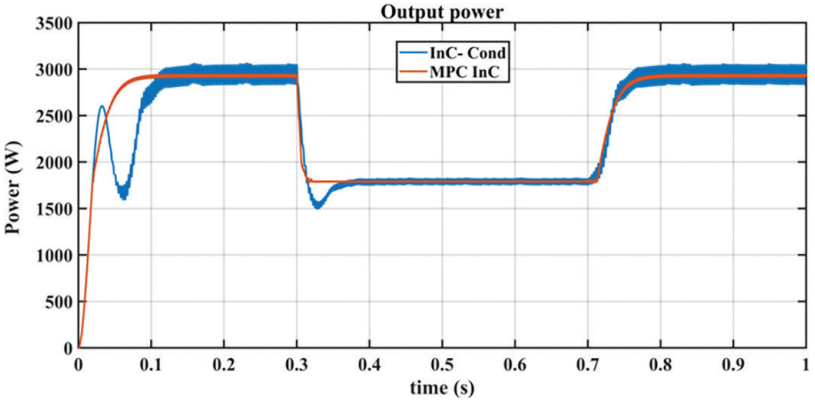

Fig. 5. Performance of MPC Inc-Cond against Inc-Cond under sudden change of illumination.

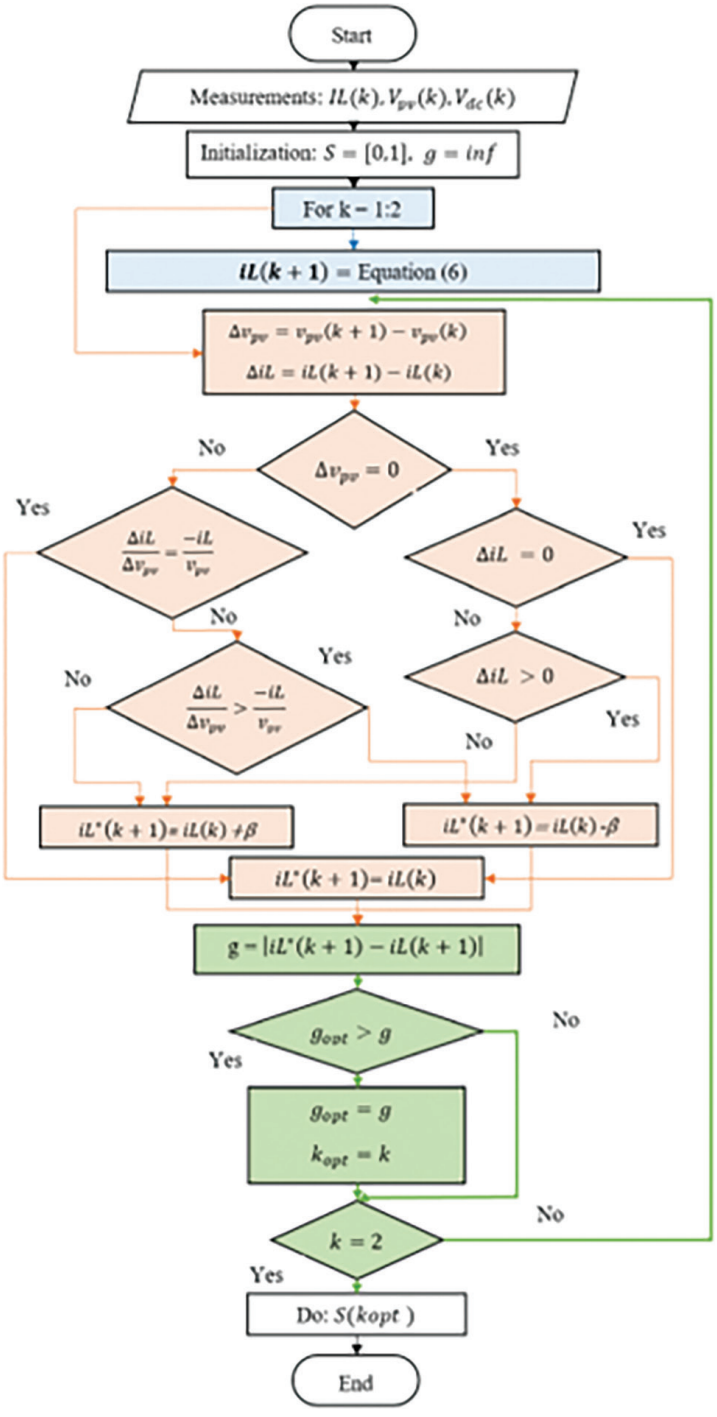

Fig. 6. Flowchart of the hybrid predictive Inc-Cond control.

levels than the conventional 2L-VSI of Figure 1. Each capacitor in the dc-link is supposed to deliver a voltage of $Vdc/4$ (Vc1 = Vc2 = Vc3 = Vc4 = Vdc/4) (Zhang et al., 2018).

Table 2 presents different output voltage levels with their respective states for the seven switches T1-…-T7. It can be noticed that there are no redundant vectors, except for the zero-voltage vector.

The different switching states of the five-level T-type inverter are summarised in the different subsections of Figure 7 for a healthy operation without faults.

Output voltage Vl	T1	T2	T3	T4	T5	T6	T7
$+v$	1	0	0	1	0	0	0
$+\frac{3v}{4}$	0	0	0	1	1	0	0
$+\frac{2v}{4}$	0	0	0	1	0	1	0
$+\frac{v}{4}$	0	0	0	1	0	0	1
0	1	1	0	0	0	0	0
0	0	0	1	1	0	0	0
$-\frac{v}{4}$	0	1	0	0	1	0	0
$-\frac{2v}{4}$	0	1	0	0	0	1	0
$-\frac{3v}{4}$	0	1	0	0	0	0	1
$-v$	0	1	1	0	0	0	0

Table 2. Possible voltage levels of the studied T-type inverter with their corresponding switching state.

2.2.2. Proposed integrated control system for grid-connected system application

The mathematical modelling of the T-type inverter is studied in this section.

The output voltage of the T-type inverter is given by the following:

$$v(t) = R_g.i_g(t) + L_g\frac{di_g}{dt} + v_g(t) \tag{8}$$

where i_g is the grid current, v_g is the grid voltage, v is the load voltage, R_g is the filter resistor, L_g is the filter inductance and Ts is the sampling time.

$$i_g(k+1) = i_g(k) + \frac{T_s}{L_g}\left[\, v(k) - v_g(k) - R_g.i_g(k)\right] \tag{9}$$

where i_g is the grid current, v_g is the grid voltage, v is the load voltage, R_g is the filter resistor, L_g is the filter inductance and Ts is the sampling time.

The output voltage of the inverter and the DC-link voltage are expressed as follows:

$$v = S_a.\left(\frac{V_{dc}}{4}\right).(S_b - S_c) \tag{10}$$

$$V_{dc} = V_{c1} + V_{c2} + V_{c3} + V_{c4} \tag{11}$$

S_a is considered the switching state of the auxiliary branch, whereas S_b and S_c are the switching states of the H-bridge legs. The variables S_a, S_b and S_c are expressed as follows:

$$S_a = \begin{cases} 1\ if\ \ T_7 = 1\ and\ \ T_5 = T_6 = 0 \\ 2\ if\ \ T_6 = 1\ and\ \ T_5 = T_7 = 0 \\ 3\ if\ \ T_5 = 1\ and\ \ T_6 = T_7 = 0 \\ \quad 4\ if\ \ T_5 = T_6 = T_7 = 0 \end{cases} \tag{12}$$

$$S_b = \begin{cases} 1\ if\ \ T_1 = 1\ and\ \ T_3 = 0 \\ 0\ if\ \ T_1 = 0\ and\ \ T_3 = 1 \end{cases} \tag{13}$$

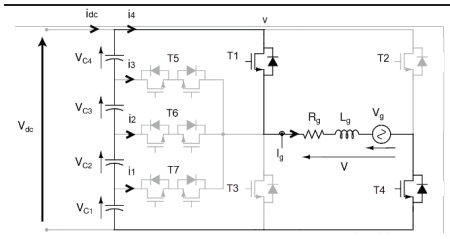

$v = v_{dc}, T_1 \text{ and } T_4 = on$

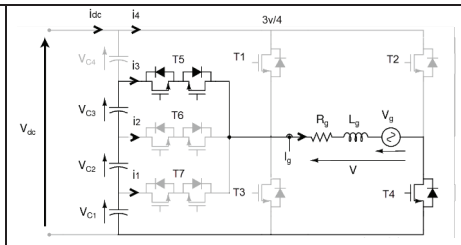

$v = 3v_{dc}/4, \ T_5 \text{ and } T_4 = on$

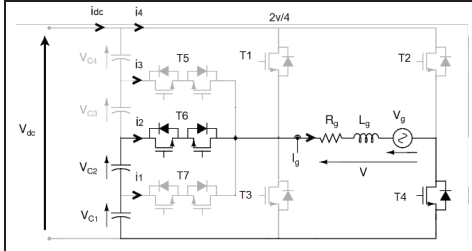

$v = v_{dc}/2, \ T_4 \text{ and } T_6 = on$

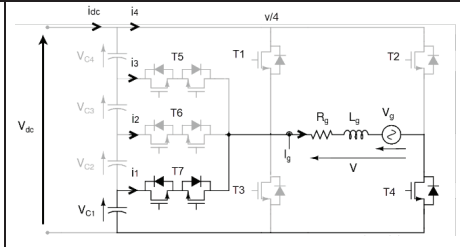

$v = v_{dc}/4, \ T_4 \text{ and } T_7 = on$

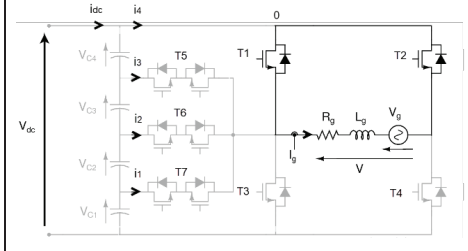

$v = 0, \ T_1 \text{ and } T_2 = on$

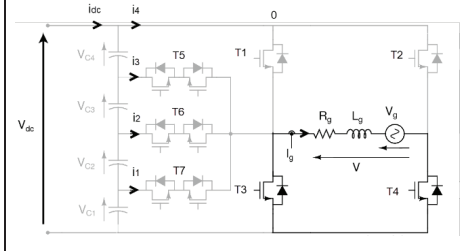

$v = 0, \ T_4 \text{ and } T_3 = on$

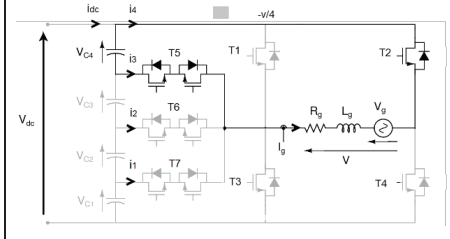

$v = -v_{dc}/4, \ T_5 \text{ and } T_2 = on$

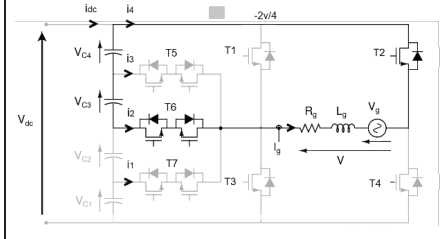

$v = -v_{dc}/2, \ T_2 \text{ and } T_6 = on$

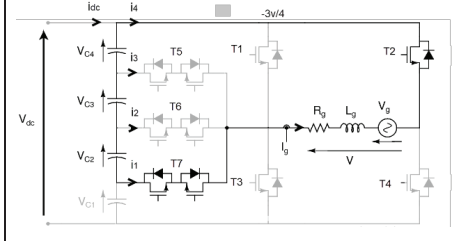

$v = -3v_{dc}/4, \ T_7 \text{ and } T_2 = on$

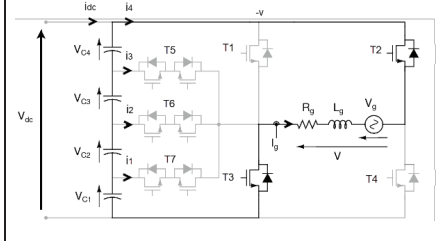

$v = -v_{dc}, \ T_3 \text{ and } T_2 = on$

Fig. 7. Different switching combinations of a five level T-type converter.

States	S_a	S_b	S_c
$+V_{dc}$	4	1	0
$+\frac{3V_{dc}}{4}$	3	1	0
$+\frac{2V_{dc}}{4}$	2	1	0
$+\frac{V_{dc}}{4}$	1	1	0
0	4	0	0
$-\frac{V_{dc}}{4}$	1	0	1
$-\frac{2V_{dc}}{4}$	2	0	1
$-\frac{3V_{dc}}{4}$	3	0	1
$-V_{dc}$	4	0	1

Table 3. Voltage levels as a function of variables S_a, S_b and S_c.

$$S_c = \begin{cases} 1 \; if \;\; T_2 = 1 \; and \;\; T_4 = 0 \\ 0 \; if \;\; T_2 = 0 \; and \;\; T_4 = 1 \end{cases} \tag{14}$$

These states are summarised in Table 3.

The capacitor voltages are expressed as follows:

$$\frac{d}{dt}\begin{bmatrix} V_{c1} \\ V_{c2} \\ V_{c3} \\ V_{c4} \end{bmatrix} = \frac{1}{C}\begin{bmatrix} i_{c1} \\ i_{c2} \\ i_{c3} \\ i_{c4} \end{bmatrix} = \frac{1}{C}\left(\begin{bmatrix} i_{c2} \\ i_{c3} \\ i_{c4} \\ i_{dc} \end{bmatrix} - \begin{bmatrix} i_1 \\ i_2 \\ i_3 \\ i_4 \end{bmatrix}\right) \tag{15}$$

After discretisation, we get

$$\begin{bmatrix} V_{c1}(k+1) \\ V_{c2}(k+1) \\ V_{c3}(k+1) \\ V_{c4}(k+1) \end{bmatrix} = \begin{bmatrix} V_{c1}(k) \\ V_{c2}(k) \\ V_{c3}(k) \\ V_{c4}(k) \end{bmatrix} + \frac{T_s}{C}\left(\begin{bmatrix} i_{c2} \\ i_{c3} \\ i_{c4} \\ i_{dc} \end{bmatrix} - \begin{bmatrix} i_1 \\ i_2 \\ i_3 \\ i_4 \end{bmatrix}\right) \tag{16}$$

Classic structures of PV grid-connected systems are generally composed of two independent control systems, as shown in Figure 1. The first one deals with the MPPT control assured by a boost chopper, whereas the second one guarantees the desired performances on the grid side. Under the FS-MPC technique, control algorithm 1 uses a simple cost function g1 of the PV current, so it is minimised for the two switching states of the considered chopper. Control algorithm 2 may include many terms such as grid current error and balance of voltage capacitors in the DC-link. The cost function g2 is then minimised for the 10 switching states of the T-type inverter. One main contribution of this study is to present an integrated topology by using only one control algorithm and an integrated cost function g that gathers all the different objectives cited earlier. Hence, the two power converters are considered an indirect matrix converter having 20 switching states, as given in Figure 8.

The two topologies of Figures 1 and 8 are then compared by the simulation to illustrate the performance of each structure. The cost function of the MPPT control is given as follows:

$$g_1 = \left| iL^*(k+1) - iL(k+1) \right| \tag{17}$$

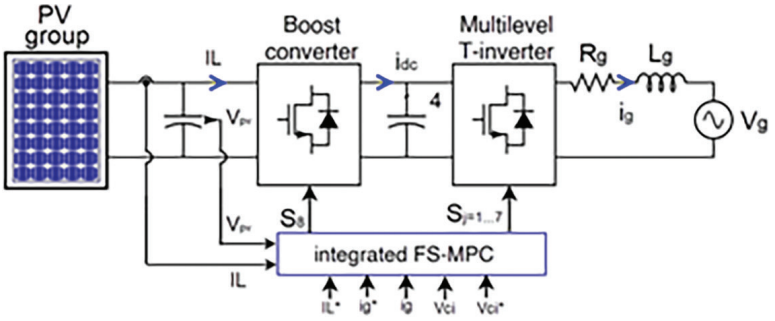

Fig. 8. Proposed integrated FS-MPC for PV-GCS.

The cost function on the grid side is given as follows:

$$g_2 = \beta \left| ig^*(k+1) - ig(k+1) \right| + \gamma \sum_{p=1}^{4} \left| (V_{dc}/4) - Vc_p(k+1) \right|^2 \tag{18}$$

The integrated cost function g is then given as follows:

$$g = \alpha \left| iL^*(k+1) - iL(k+1) \right| + \beta \left| ig^*(k+1) - ig(k+1) \right| + \gamma \sum_{p=1}^{4} \left| (V_{dc}/4) - Vc_p(k+1) \right|^2 \tag{19}$$

Other objectives can be added such as switching numbers:

$$g = \alpha \left| iL^*(k+1) - iL(k+1) \right| + \beta \left| ig^*(k+1) - ig(k+1) \right| + \gamma \sum_{p=1}^{4} \left| (V_{dc}/4) - Vc_p(k+1) \right|^2 + \mu N_{sw} \tag{20}$$

where α, β, γ and μ are weighting factors (Cortes et al., 2009).

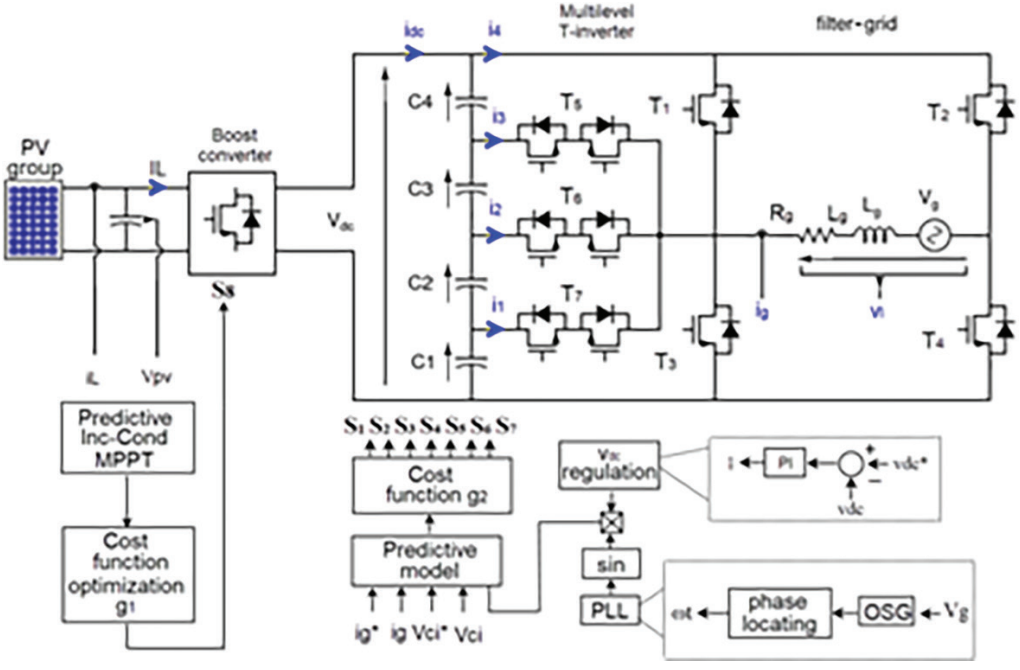

Fig. 9. Control scheme of the generic PVGCS using FS-MPC.

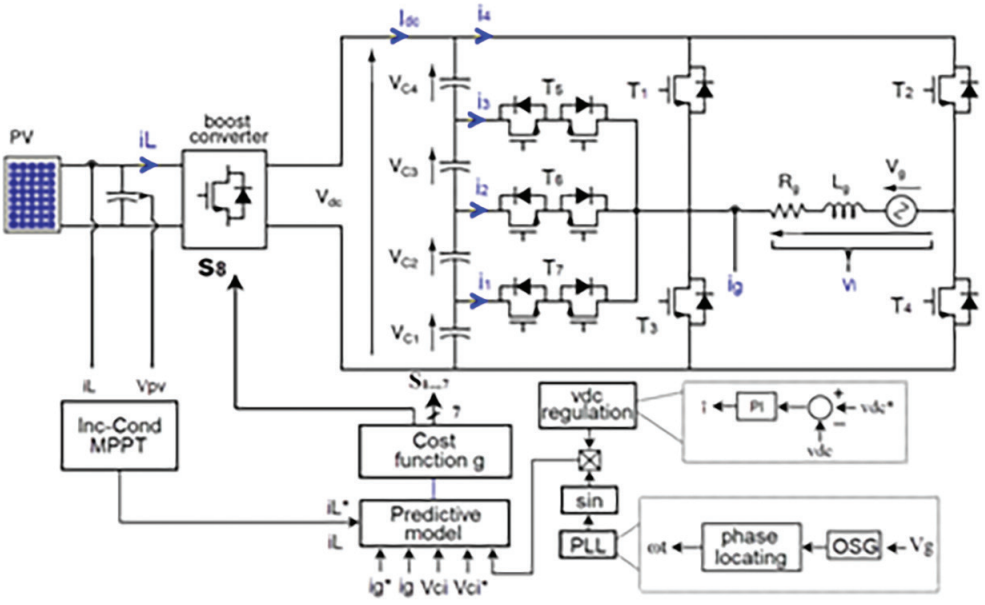

Fig. 10. Control scheme of the proposed PVGCS using FS-MPC.

Parameter	Value
PV	300 W
Group PV (5×2)	3 kW
Current at MPP	8.1 A
Voltage at MPP	36.7 V
Capacitor boost input C	3 µF
Capacitor dc link $C_{1,2,3,4}$	4.5 mF
Inductor *L*	25 mH
Filter inductor L_g	3.5 mH
Internal inductor resistor R_g	0.1 Ω
Grid RMS voltage V_g	220 V
Sampling time T_s	30 µs

Table 4. Parameters of the on-grid PV system.

The switching number is given as follows:

$$N_{sw} = \sum_{n=1}^{7} \left| S_n(k) - S_n(k-1) \right| \tag{21}$$

$$N_{sw} = \sum_{n=1}^{8} \left| S_n(k) - S_n(k-1) \right| \tag{22}$$

where Eq. (21) refers to the separated case, whereas Eq. (22) represents the integrated case (Figures 9 and 10) respectively.

2.3. Results and discussion

To well illustrate the performance of the proposed integrated control system IFS-MPC over the classic control FS-MPC, a series of simulation results under Matlab-Simulink software have been carried out using the same values of the power circuit parameters listed in the Table 4 (the same conditions of simulation).

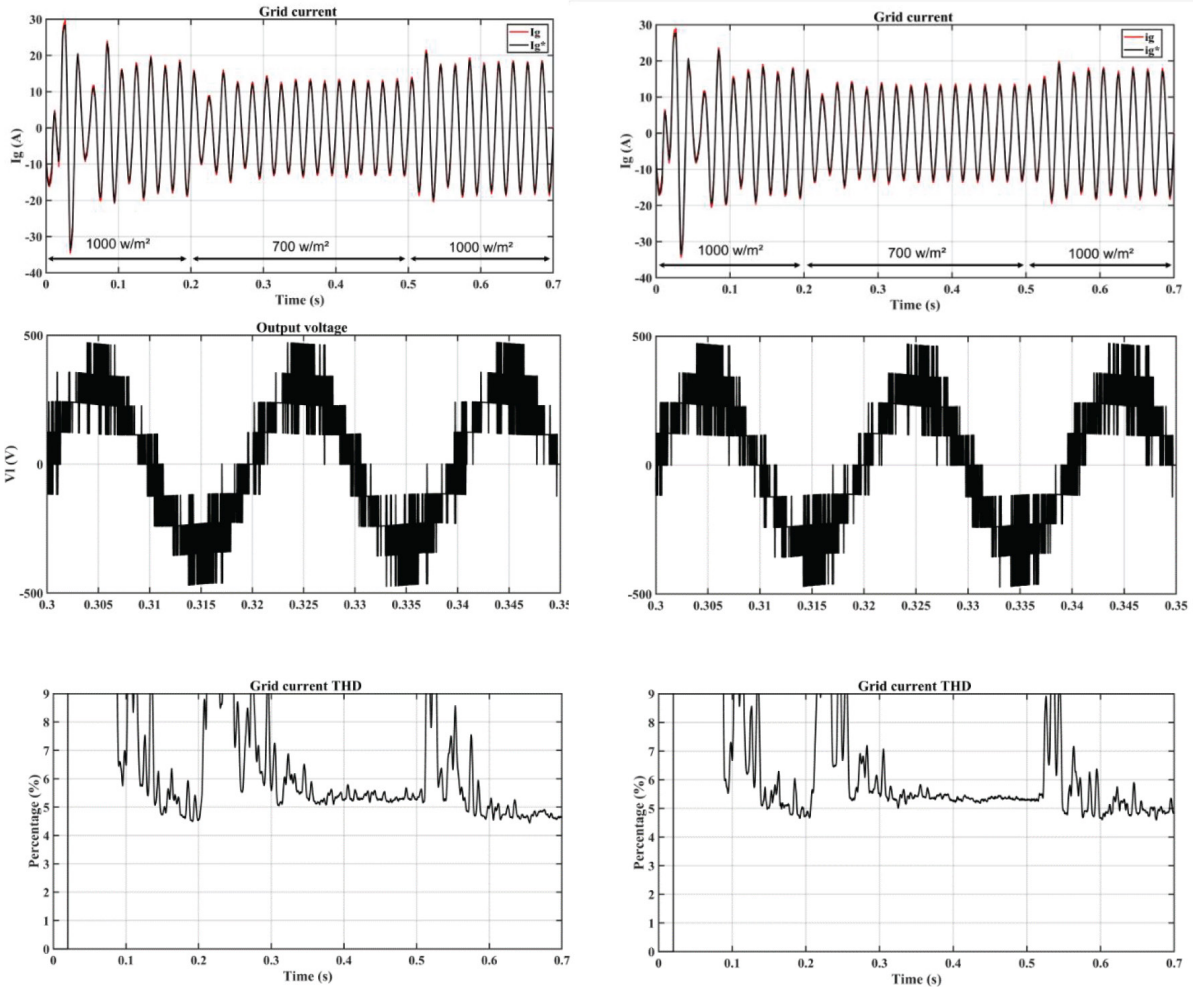

Fig. 11. Simulation results for separated and integrated FS-MPC (DC-link capacitor regulation, grid current and output voltage with grid current THD). FS-MPC, finite set-model predictive control.

Figure 11 depicts the separated strategy on the right, while the integrated control strategy IFS-MPC is depicted on the left. The various sizes are simulated for three profiles of irradiation [1,000-700-1,000] W/m². For dc-link voltage regulation V_{dc} and grid current i_g, the results are quite similar for the steady state as for the transient state. For the output voltage vl and grid current total harmonic distortion (THD), we notice similar results in both transient and steady states. This means that integrating the cost functions of the two FS-MPCs to reduce the size of calculating hardware does not negatively affect the performance of the system.

2.3.1. Faulty operation of the grid-connected PV system

Grid-tied PV systems are sometimes subject to certain faults in converter components such as power switches or DC bus capacitors (Chai et al., 2020; Lezana et al., 2010; Sebaaly et al., 2021; Wang et al., 2020). To preserve the correct functioning of the PVGCS respecting the grid connection criteria under faulty conditions and to guarantee an appreciable quality of energy during this operation, we propose a modified control algorithm design called M-IFS-MPC.

Two scenarios are examined, when one of the DC-link capacitors fails and when one of the auxiliary switches breaks down. This design permits the inverter to switch at any time between five and four levels mode of operation without any intervention on the power circuit level.

Scenario 1

Usually, DC-link comprises at least a single capacitor or more. The choice of these capacitors is not limited only to electric parameter sizing. It also depends on many other factors, such as the environment, exposure to extreme

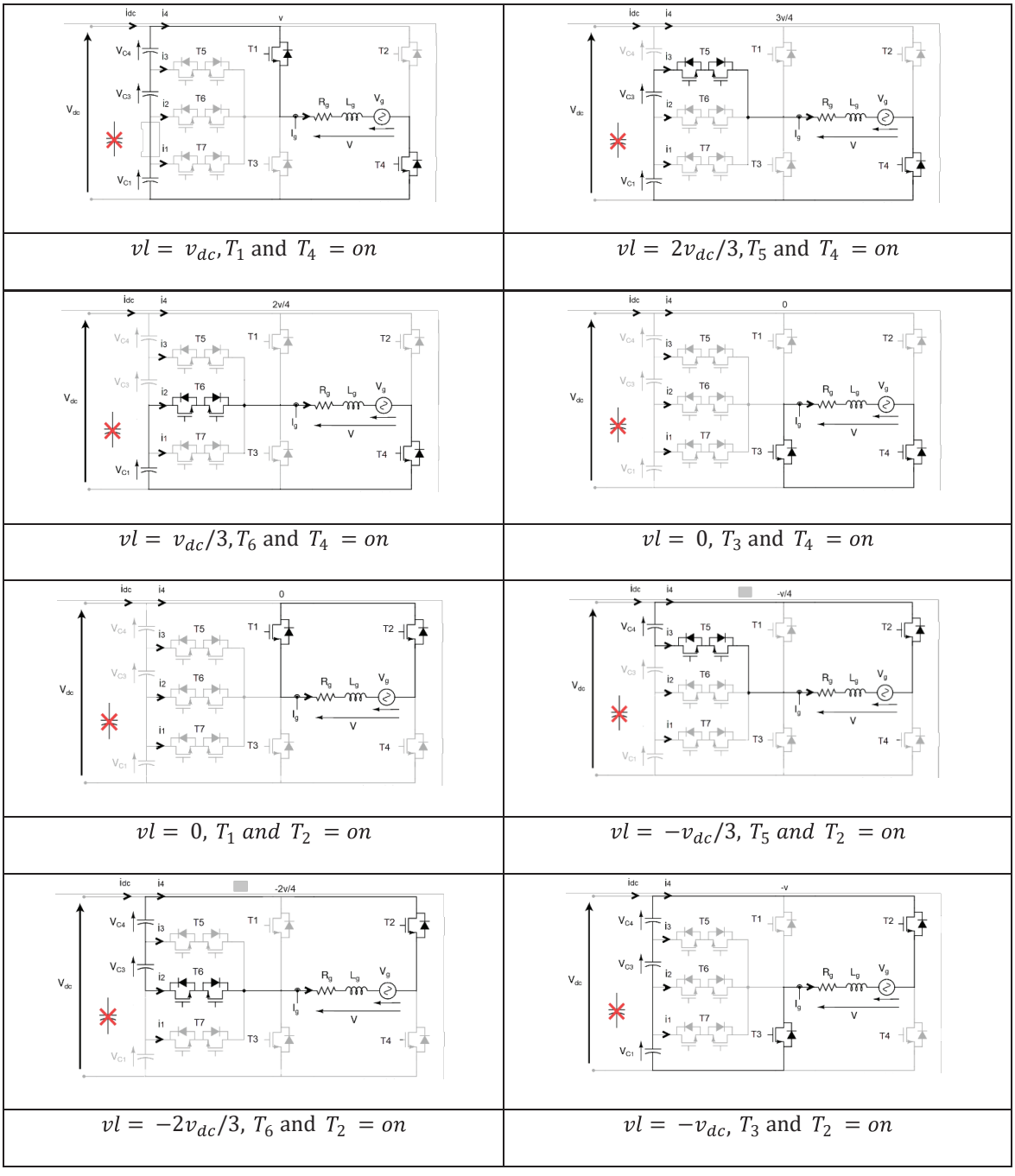

Fig. 12. Operating phases when a short-circuited capacitor in the DC-link happens.

conditions (ambient temperature, humidity, etc.) and constraints on power density applications. Thus, depending on the type of capacitor, we distinguish three modes of failure: open circuit failure, short circuit failure and wear-out failure. Short circuit failure is the most fault mode for DC link capacitors that can happen, so it is considered in the present study (Rao Mucherla et al., 2022; Wang and Blaabjerg, 2014).

In the present study, we consider short-circuit failure that is detected by using the voltage sensors dedicated to the voltage balancing procedure. In an ideal short-circuit case, the voltage drops to zero. This latter is coded as a condition in the control algorithm, which decides whether to work in a five-level or four-level mode of operation.

Scenario 1 supposes that a DC link capacitor (C2) is short-circuited at 0.3 s, so vc2 = 0. The functioning of the T-type inverter is now modified, so the logic variable of the auxiliary branch S_{a1}" becomes as follows:

$$S_{a1}' = \begin{cases} 1 \; if \;\; T_6 = 1 \text{ and } T_5 = 0 \\ 2 \; if \;\; T_5 = 1 \text{ and } T_6 = 0 \\ 3 \; if \;\; T_5 = T_6 = 0 \end{cases} \tag{23}$$

$$S_b = \begin{cases} 1 \; if \;\; T_1 = 1 \text{ and } T_3 = 0 \\ 0 \; if \;\; T_1 = 0 \text{ and } T_3 = 1 \end{cases} \tag{24}$$

$$S_c = \begin{cases} 1 \; if \;\; T_2 = 1 \text{ and } T_4 = 0 \\ 0 \; if \;\; T_2 = 0 \text{ and } T_4 = 1 \end{cases} \tag{25}$$

The inverter output voltage is as follows:

$$vl = S_{a1}' \left(\frac{V_{dc}}{3} \right) \left(S_b - S_c \right) \tag{26}$$

Finally, the Dc-link voltage is given as follows:

$$V_{dc} = V_{c1} + V_{c3} + V_{c4} \tag{27}$$

The different operating phases of the inverter are now eight (8) in number, instead of 10, and are summarised in Figure 12.

The output voltage levels are now four (Vdc, 2Vdc/3, Vdc/3, 0), instead of five, and are given in Table 5.

Scenario 2

Regarding power switches, generally, we have two modes of failure: open-circuit fault and short-circuit fault (Wu et al., 2013). In the present study, the unhealthy studied case is the open-circuit failure. A load voltage sensor is used to detect the presence/absence of the voltage level; therefore, an open-circuit failure is detected by the absence of a certain voltage level, in our case vc1. When the algorithm detects the failure, it decides to segregate the faulty switch and change the functioning from a five-level to a four-level operation. Let us examine a complicated assumption when two combined faults occur simultaneously. A short circuit of the capacitor C2 occurs at 0.2 s (Scenario 1), followed by a failure of the switch T6 at 0.6 s.

State	S_{a1}'	S_b	S_c
$+V_{dc}$	3	1	0
$+\frac{2V_{dc}}{3}$	2	1	0
$+\frac{V_{dc}}{3}$	1	1	0
0	3	0	0
$-\frac{V_{dc}}{3}$	1	0	1
$-\frac{2V_{dc}}{3}$	2	0	1
$-V_{dc}$	3	0	1

Table 5. Different output voltage levels for Scenario 1.

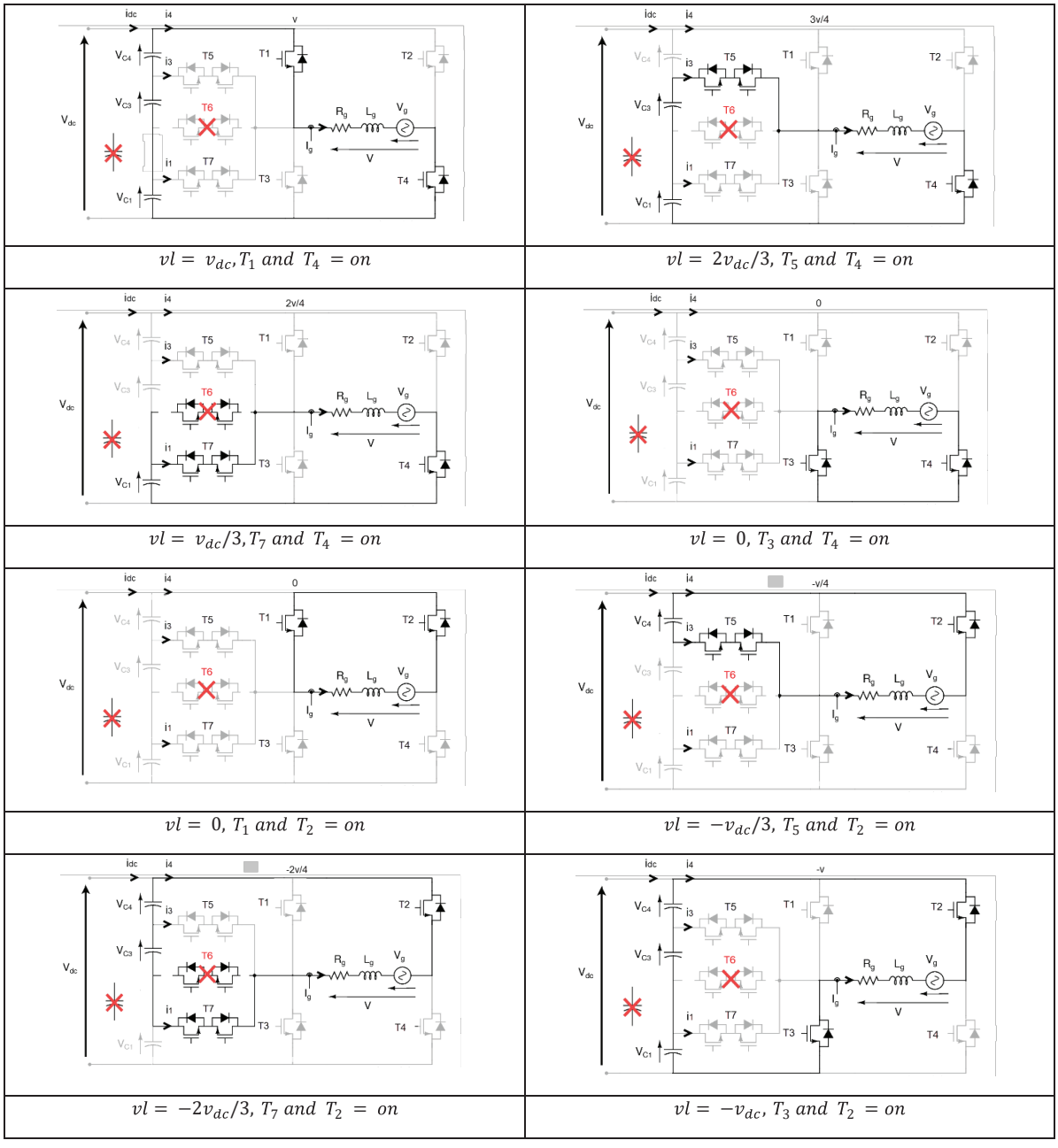

Fig. 13. Operating phases of the converter under combined faults.

Under these assumptions, the inverter has to switch between five- and four-level modes. The functioning of the T-type inverter is now modified, so the logic variable of the auxiliary branch, and S_{a2}' becomes as follows:

$$S_{a2}' = \begin{cases} 1 \text{ if } T_7 = 1 \text{ and } T_5 = 0 \\ 2 \text{ if } T_5 = 1 \text{ and } T_7 = 0 \\ 3 \text{ if } T_5 = T_7 = 0 \end{cases} \quad (28)$$

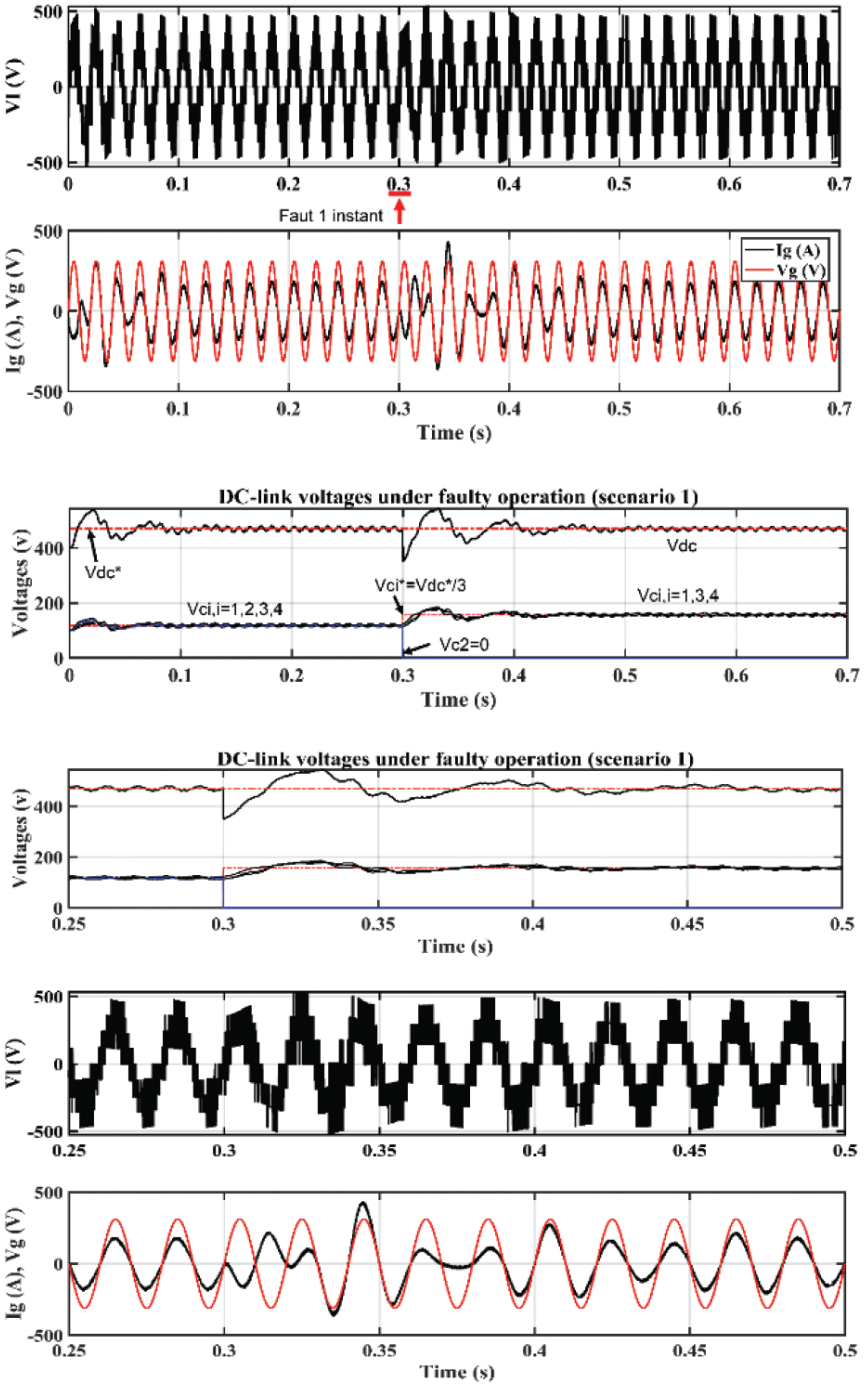

Fig. 14. Results for Scenario 1 (DC-link capacitor short-circuited): Output voltage, voltage and grid current, DC-link voltages with their zoom.

$$S_b = \begin{cases} 1 \text{ if } T_1 = 1 \text{ and } T_3 = 0 \\ 0 \text{ if } T_1 = 0 \text{ and } T_3 = 1 \end{cases} \tag{29}$$

$$S_c = \begin{cases} 1 \text{ if } T_2 = 1 \text{ and } T_4 = 0 \\ 0 \text{ if } T_2 = 0 \text{ and } T_4 = 1 \end{cases} \tag{30}$$

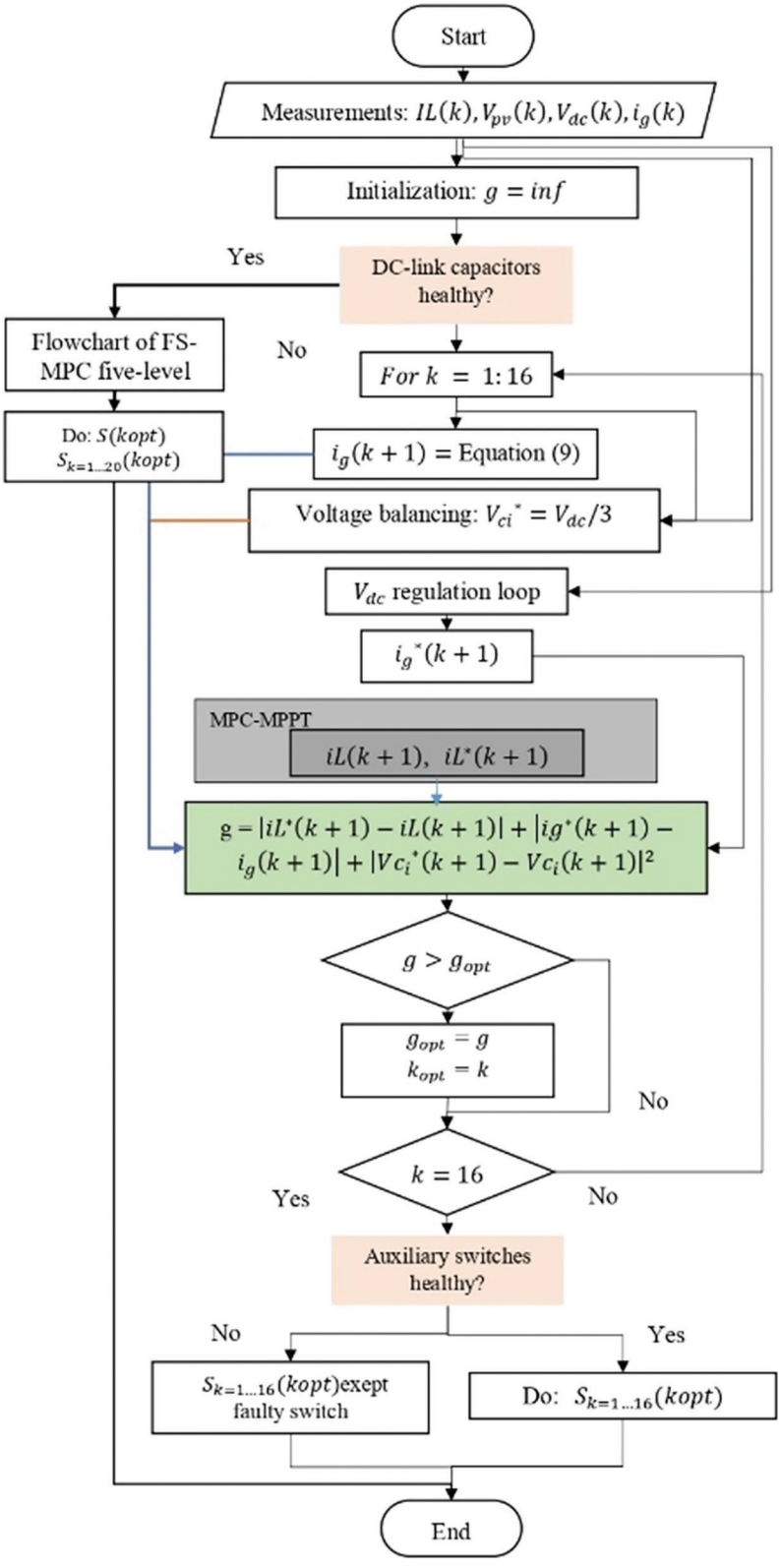

Fig. 15. Flowchart of the proposed M-IFS-MPC for the faulty mode of the power converter.

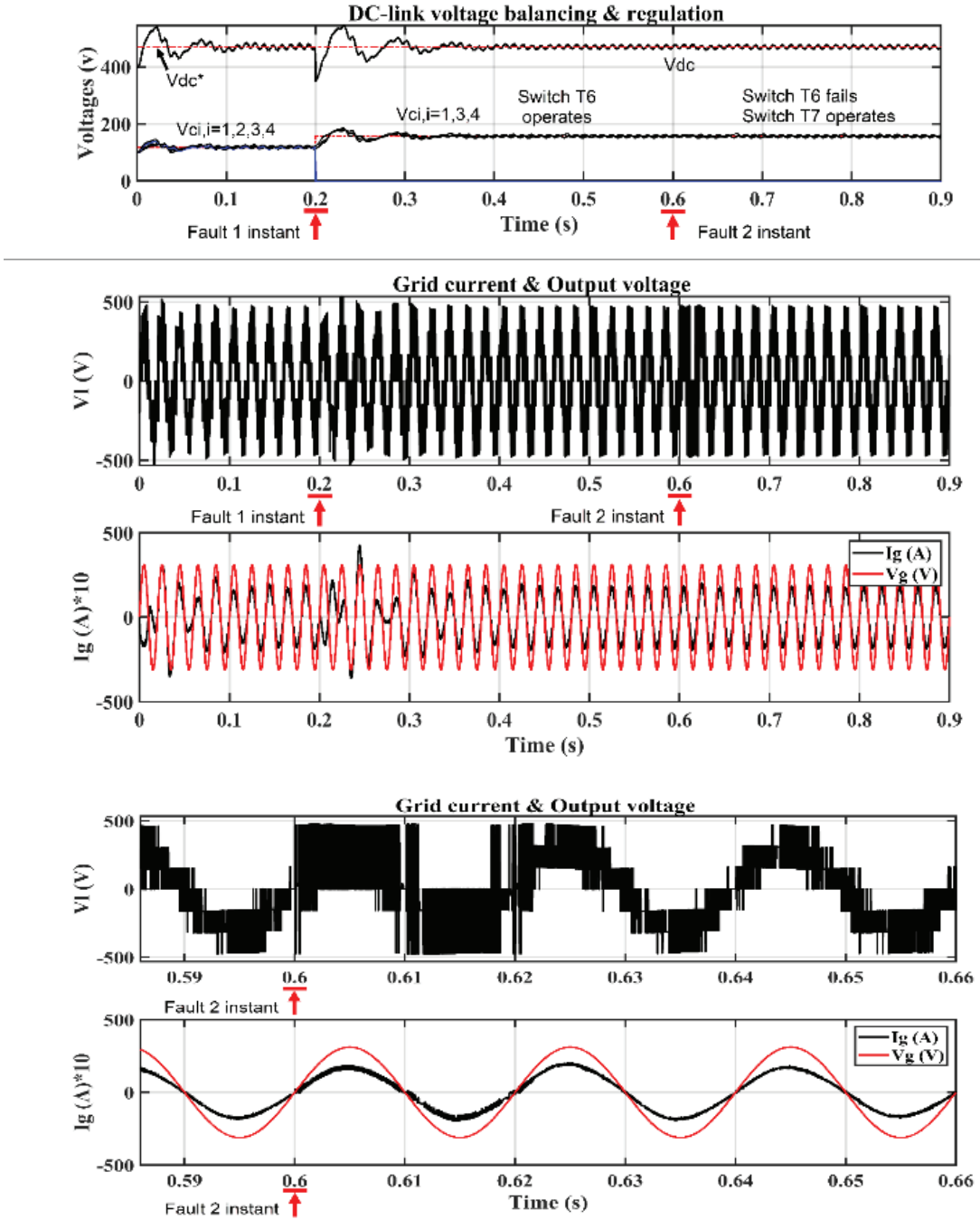

Fig. 16. Simulation results for Scenario 2: DC-link voltages, output inverter voltage, voltage and grid current with their zoom.

The inverter output voltage becomes as follows:

$$vl = S_{a2}{}'\left(\frac{V_{dc}}{3}\right)\left(S_b - S_c\right) \tag{31}$$

The output voltage levels are now four (Vdc, 2Vdc/3, Vdc/3, 0), instead of five. The different operating voltages of the inverter are also eight (8) and are summarised in Figure 13.

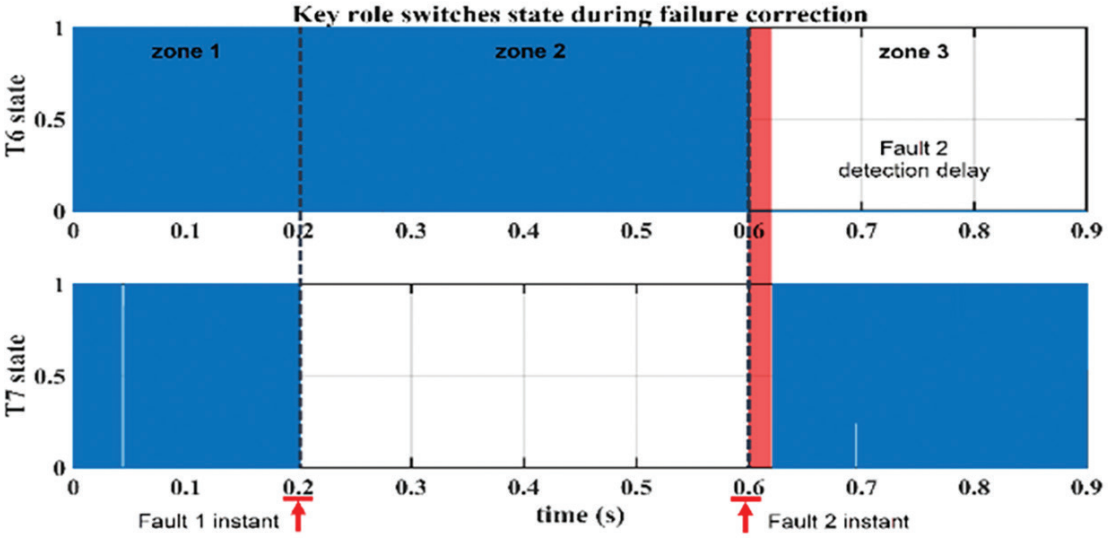

Fig. 17. Key role switches state during failure correction.

Finally, the Dc-link voltage is given as follows:

$$V_{dc} = V_{c1} + V_{c3} + V_{c4} \tag{32}$$

To ensure the proper functioning of the PVGCS under the different types of faults considered in the present study, a modified algorithm is performed called M-IFS-MPC. The main idea of the proposed algorithm is to keep the DC-link voltage Vdc constant for both healthy and faulty modes. When a fault is detected in the converter, a new reference voltage is generated for each capacitor of the DC-link to keep the global DC-link voltage constant. In our study, for the healthy mode, Vci* = Vdc/4, but when a capacitor is short-circuited in the converter, a new reference voltage for each healthy capacitor is now generated as Vci* = Vdc/3. This switched mode will procure the PVGCS, a high-power quality in terms of low THD and unity power factor functioning. The proposed algorithm is illustrated in Figure 15, where the global cost function is now minimised for 16 switching states, instead of 20 in the healthy case.

Figure 15 shows the flowchart of M-FS-MPC that takes into account the healthy operation as well as the fault rejection operation. If a healthy operation is running, the five-level FS-MPC algorithm is used. At each instant k, the sizes iL(k), $V_{pv}(k)$, $V_{dc}(k)$, $i_g(k)$ are measured. Furthermore, at every instant k, the algorithm tests if a fault has occurred in both the DC-link capacitors and the auxiliary switches. This test is performed without adding external hardware components, that is, using the DC-link capacitors' voltage balancing sensors, in addition to the inverter output voltage sensor. If a four-level voltage operation is detected due to a failure in the capacitor of the dc-link (i.e., capacitor 2 in Scenario 1), a new reference voltage for each capacitor of the DC-link is generated to keep the global DC-link voltage constant. The reference value of V_{dc} remains the same; however, the reference value of each capacitor is chosen as one-third of the dc-link voltage. The MPPT algorithm generates the inductor current reference iL, which will be optimized in the cost function along with the grid current i_g as well as the DC-link capacitors' voltages. Finally, once the voltage vector is chosen, the algorithm takes less than one period to perform its second test to determine whether the auxiliary switches are properly operating or not. If one of the auxiliary switches (i.e., switch 6 in Scenario 2) is broken, the algorithm chooses another combination of switches to generate the same voltage vector already selected after cost function g optimisation. The overall proposed algorithm is very simple. It just needs voltage sensors both in the DC link side (for each capacitor) and a voltage sensor on the load side. The sensors are used to detect and locate the failure then the developed algorithm intervein for the decision on the system operation.

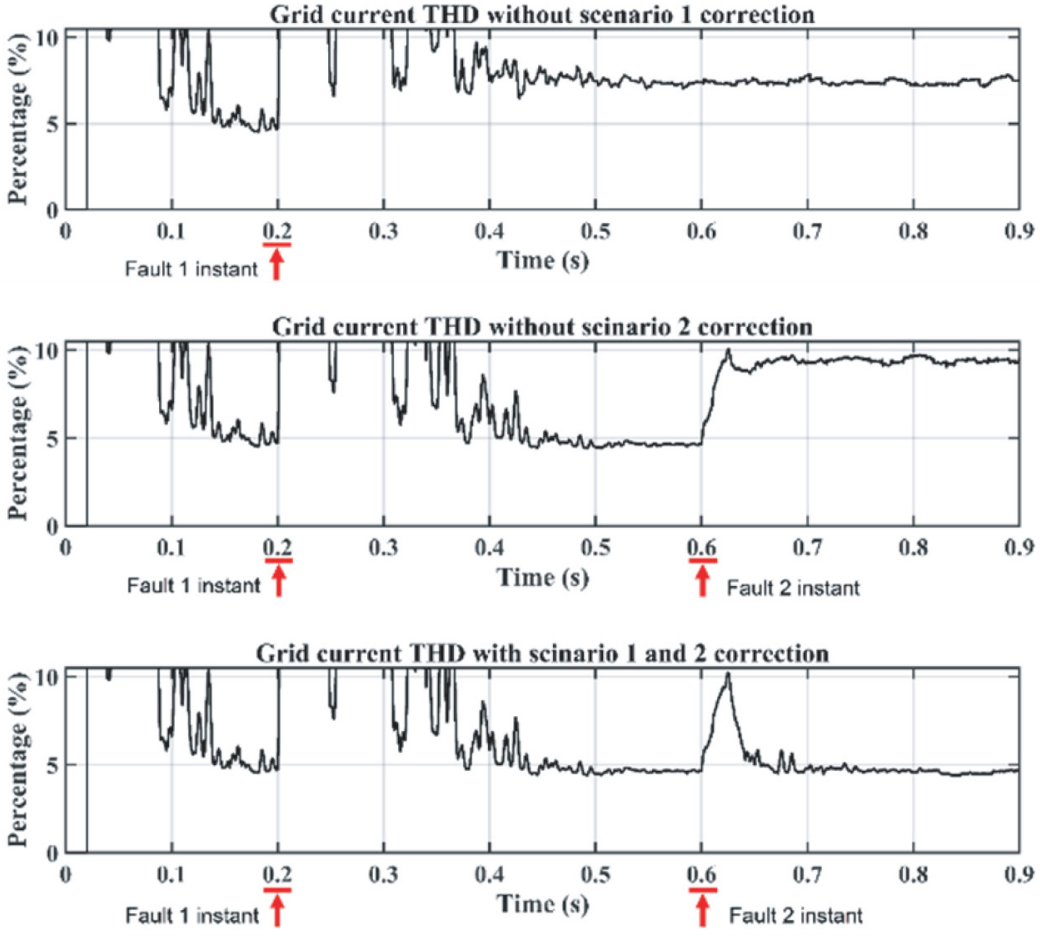

Fig. 18. Impact of the M-IFS-MPC on grid current THD: (a) without Scenario 1 correction. (b) without Scenario 2 correction. (c) under M-IFS-MPC correction.

2.4. Simulation results under faulty conditions

Scenario 1

The first set of simulation results of the PVGCS is displayed in Figure 14 when one of the DC-link capacitors is short-circuited at 0.3 s. The control system operates in the healthy mode in the range [0–0.3] s with five-level mode of the converter. In this range, the four voltage capacitors are balanced, and the system works normally at unity power factor. At t = 0.3 s, we assume that the second capacitor is short-circuited (Vc2 = 0), causing a transient state for the DC-link voltage. As can be seen, the modified algorithm M-IFS-MPC operates now and will generate a new reference voltage for each healthy capacitor to keep the global DC-link voltage close to its initial value of 440 V, so, $V_{ci}^{*} = 440/3$ V, instead of 440/4 V. During this transient state, the inverter output voltage switches from the five-level mode to the four-level mode without affecting the output power quality injected into the grid since the system returns to its state before the fault by working at unity power factor, as illustrated by the zoomed region.

Scenario 2

This scenario is displayed by the set of simulation results depicted in Figure 16. We assume that a short circuit of the capacitor C2 occurs at 0.2 s (as in Scenario 1 case), followed by a failure of the auxiliary branch switch T6 at 0.6 s. The operating profile of the considered system can then be subdivided into three zones. In [0–0.2] s, the system is healthy, and the inverter operates with the five-level mode at unity power factor with 5% THD for the grid

current in the steady state. In [0.2–0.6] s, Scenario 1 occurs, and the modified M-IFS-MPC becomes operational, so the inverter switches from the five-level mode to the four-level mode without affecting the output power quality on the grid side. At t = 0.6 s, a combined fault happens due to a breakdown of switch T6. Then, the inverter tends to lose its voltage levels, as shown in the red zone [0.6 – 0.62] s of Figure 17 before recovering them at t = 0.62 s, thanks to the switch T7, which comes into conduction after a delay of one period, as shown by Figure 16. Beyond 0.62 s, the inverter recovers its four voltage levels without affecting the injected power quality.

To well illustrate the impact of the M-IFS-MPC under faulty functioning of the PVGCS respecting the grid current THD, Figure 18 illustrates the grid current THD for both scenarios. At first, in the healthy zone, the THD is around 5% in the steady state; beyond the fault1 instant, the THD becomes around 7.5% in the steady state without correction but jumps down to 5% when M-IFS-MPC is activated. When the combined fault occurs (at 0.6 s), the THD climbs to 9.5% without correction but falls to 5% when activating the M-IFS-MPC algorithm.

3. Conclusion

The article presents two contributions for PVGCSs. The first contribution is an optimised predictive control called IFS-MPC, which has the merit of controlling cascaded power converter structures in one stage as an indirect matrix converter. The boost converter and the T-type inverter are controlled at the same time using only one cost function, instead of controlling them separately, so the control circuit of the system is greatly reduced. The performance of the IFS-MPC is revealed via simulation, which showed that high dynamic and static performance can be achieved as in the case when controlling them separately without affecting the power quality on the grid side.

The second part of the article treats the extension of the proposed design to systems operating under converter faults. A modified M-IFS-MPC is developed to cope with the different faults, which can occur in the inverter branches, such as a short circuit of a DC-link capacitor and a failure of a branch switch.

The three terms of the cost function are chosen meticulously to fulfil the requirements of the PVGCS. The proposed design for both healthy and faulty systems permits switching at any time from a five-level mode to a four-level mode of operation by a proper selection of the auxiliary DC-link voltage without degradation of the power quality on the grid side and intervention on the hardware level. The obtained results of the M-IFS-MPC are excellent for both static and dynamic behaviour of the controlled system and prove that this latter can be used efficiently under faulty conditions of power converters. These results are to be further confirmed in future works through a practical realisation.

References

Abu-Rub, H., Holtz, J., Rodriguez, J. and Baoming, G. (2010). Medium-Voltage Multilevel Converters – State of the Art, Challenges, and Requirements in Industrial Applications. *IEEE Transactions on Industrial Electronics*, 57, pp. 2581–2596. doi: 10.1109/TIE.2010.2043039.

Acharya, A. B., Ricco, M., Sera, D., Teoderscu, R. and Norum, L. E. (2019). Performance Analysis of Medium-Voltage Grid Integration of PV Plant using Modular Multilevel Converter. *IEEE Transactions on Energy Conversion*, 34, pp. 1731–1740. doi: 10.1109/TEC.2019.2930819.

Arikesh, A. and Parvathy, A. K. (2020). Modular Multilevel Inverter for Renewable Energy Applications. *International Journal of Electrical and Computer Engineering*, 10, p. 1. doi: 10.11591/ijece.v10i1.pp1-14.

Azer, P., Ouni, S. and Narimani, M. (2020). A Novel Fault-Tolerant Technique for Active-Neutral-Point-Clamped Inverter Using Carrier-Based PWM. *IEEE Transactions on Industrial Electronics*, 67, pp. 1792–1803. doi: 10.1109/TIE.2019.2903764.

Bughneda, A., Salem, M., Richelli, A., Ishak, D. and Alatai, S. (2021). Review of Multilevel Inverters for PV Energy System Applications. *Energies*, 14, p. 1585. doi: 10.3390/en14061585.

Ceglia, G., Guzman, V., Sanchez, C., Ibanez, F., Walter, J. and Gimenez, M. I. (2006). A New Simplified Multilevel Inverter Topology for DC–AC Conversion. *IEEE Transactions on Power Electronics*, 21, pp. 1311–1319. doi: 10.1109/TPEL.2006.880303.

Chai, M., Gorla, N. B. Y. and Panda, S. K. (2020). Fault Detection and Localization for Cascaded H-Bridge Multilevel Converter with Model

Predictive Control. *IEEE Transactions on Power Electronics*, 35, pp. 10109–10120. doi: 10.1109/TPEL.2020.2978670.

Cortes, P., Kouro, S., La Rocca, B., Vargas, R., Rodriguez, J., Leon, J. I., Vazquez, S. and Franquelo, L. G. (2009). Guidelines for weighting factors design in model predictive control of power converters and drives. *In: 2009 IEEE International Conference on Industrial Technology. Presented at the 2009 IEEE International Conference on Industrial Technology – (ICIT)*, Churchill, Victoria, Australia: IEEE, pp. 1–7. doi: 10.1109/ICIT.2009.4939742.

Franquelo, L., Rodriguez, J., Leon, J., Kouro, S., Portillo, R. and Prats, M. (2008). The Age of Multilevel Converters Arrives. *IEEE Industrial Electronics Magazine*, 2, pp. 28–39. doi: 10.1109/MIE.2008.923519.

Gupta, K. K., Ranjan, A., Bhatnagar, P., Sahu, L. K. and Jain, S. (2016). Multilevel Inverter Topologies with Reduced Device Count: A Review. *IEEE Transactions on Power Electronics*, 31, pp. 135–151. doi: 10.1109/TPEL.2015.2405012.

Huang, J. and Corzine, K. A. (2006). Extended Operation of Flying Capacitor Multilevel Inverters. *IEEE Transactions on Power Electronics*, 21, pp. 140–147. doi: 10.1109/TPEL.2005.861108.

Karami, N. (2017). General Review and Classification of Different MPPT Techniques. *Renewable and Sustainable Energy Reviews*, pp. 1–18. doi: 10.1016/j.rser.2016.09.132.

Kouro, S., Malinowski, M., Gopakumar, K., Pou, J., Franquelo, L. G., Wu, B., Rodriguez, J., Pérez, M. A. and Leon, J. I. (2010). Recent Advances and Industrial Applications of Multilevel Converters. *IEEE Transactions on Industrial Electronics*, 57, pp. 2553–2580. doi: 10.1109/TIE.2010.2049719.

Lezana, P., Pou, J., Meynard, T. A., Rodriguez, J., Ceballos, S. and Richardeau, F. (2010). Survey on Fault Operation on Multilevel Inverters. *IEEE Transactions on Industrial Electronics*, 57, pp. 2207–2218. doi: 10.1109/TIE.2009.2032194.

Meddour, S., Rahem, D., Wira, P., Laib, H., Cherif, A. Y. and Chtouki, I. (n.d). Design and Implementation of an Improved Metaheuristic Algorithm for Maximum Power Point Tracking Algorithm Based on a PV Emulator and a Double-Stage Grid-Connected System 9. pp. 123-131. doi: 10.18280/ejee.240301

Ouchatti, A., Majdoul, R., Moutabir, A., Taouni, A. and Touati, A. (2022). Modified T-Type Topology of Three-Phase Multi-Level Inverter for Photovoltaic Systems. *International Journal of Electrical and Computer Engineering*, 12, p. 262. doi: 10.11591/ijece.v12i1.pp262-268.

Ounejjar, Y., Al-Haddad, K. and Grégoire, L. -A. (2011). Packed U Cells Multilevel Converter Topology: Theoretical Study and Experimental Validation. *IEEE Transactions on Industrial Electronics*, 58, pp. 1294–1306. doi: 10.1109/TIE.2010.2050412.

Peyghami, S., Palensky, P. and Blaabjerg, F. (2020). An Overview on the Reliability of Modern Power Electronic Based Power Systems. *IEEE Open Journal of Power Electronics*, 1, pp. 34–50. doi: 10.1109/OJPEL.2020.2973926.

Rao Mucherla, N., Karthick, N. and Rao, A. M. (2022). Fault Tolerant Nine-Level Inverter Topology for Solar Water Pumping Applications. *International Journal of Electrical and Computer Engineering*, 12, p. 3485. doi: 10.11591/ijece.v12i4.pp3485-3493.

Remache, S. E. I., Cherif, A. Y. and Barra, K. (2019). Optimal Cascaded Predictive Control for Photovoltaic Systems: Application Based on Predictive Emulator. *IET Renewable Power Generation*, 13, pp. 2740–2751. doi: 10.1049/iet-rpg.2019.0068.

Rezaei, M. A., Nayeripour, M., Hu, J., Band, S. S., Mosavi, A. and Khooban, M. -H. (2022). A New Hybrid Cascaded Switched-Capacitor Reduced Switch Multilevel Inverter for Renewable Sources and Domestic Loads. *IEEE Access*, 10, pp. 14157–14183. doi: 10.1109/ACCESS.2022.3146256.

Riera-Guasp, M., Antonino-Daviu, J. A. and Capolino, G.-A. (2015). Advances in Electrical Machine, Power Electronic, and Drive Condition Monitoring and Fault Detection: State of the Art. *IEEE Transactions on Industrial Electronics*, 62, pp. 1746–1759. doi: 10.1109/TIE.2014.2375853.

Rodriguez, J., Bernet, S., Steimer, P. K. and Lizama, I. E. (2010). A Survey on Neutral-Point-Clamped Inverters. *IEEE Transactions on Industrial Electronics*, 57, pp. 2219–2230. doi: 10.1109/TIE.2009.2032430.

Rodriguez, J., Lai, J. -S. and Peng, F. Z. (2002). Multilevel Inverters: A Survey of Topologies, Controls, and Applications. *IEEE Transactions on Industrial Electronics*, 49, pp. 724–738. doi: 10.1109/TIE.2002.801052.

Sebaaly, F., Sharifzadeh, M., Kanaan, H. Y. and Al-Haddad, K. (2021). Multilevel Switching-Mode Operation of Finite-Set Model Predictive Control for Grid-Connected Packed E-Cell Inverter. *IEEE Transactions on Industrial Electronics*, 68, pp. 6992–7001. doi: 10.1109/TIE.2020.3003627.

Sharifzadeh, M. and Al-Haddad, K. (2019). Packed E-Cell (PEC) Converter Topology Operation and Experimental Validation. *IEEE Access*, 7, pp. 93049–93061. doi: 10.1109/ACCESS.2019.2924009.

Vazquez, S., Rodriguez, J., Rivera, M., Franquelo, L. G. and Norambuena, M. (2017). Model Predictive Control for Power Converters and Drives: Advances and Trends. *IEEE Transactions on Industrial Electronics*, 64, pp. 935–947. doi: 10.1109/TIE.2016.2625238.

Vemuganti, H. P., Sreenivasarao, D., Ganjikunta, S. K., Suryawanshi, H. M. and Abu-Rub, H. (2021). A Survey on Reduced Switch Count Multilevel Inverters. *IEEE Open Journal of the Industrial Electronics Society*, 2, pp. 80–111. doi: 10.1109/OJIES.2021.3050214.

Villanueva, E., Correa, P., Rodriguez, J. and Pacas, M. (2009). Control of a Single-Phase Cascaded H-Bridge Multilevel Inverter for Grid-Connected Photovoltaic Systems. *IEEE Transactions on Industrial Electronics*, 56, pp. 4399–4406. doi: 10.1109/TIE.2009.2029579.

Wang, H. (n.d). Design for Reliability of Power Electronic Systems.

Wang, H. and Blaabjerg, F. (2014). Reliability of Capacitors for DC-Link Applications in Power Electronic Converters – An Overview. *IEEE Transactions on Industry Applications*, 50, pp. 3569–3578. doi: 10.1109/TIA.2014.2308357.

Wang, B., Li, Z., Bai, Z., Krein, P. T. and Ma, H. (2020). A Redundant Unit to Form T-Type Three-Level Inverters Tolerant of IGBT Open-Circuit Faults in Multiple Legs. *IEEE Transactions on Power Electronics*, 35, pp. 924–939. doi: 10.1109/TPEL.2019.2912177.

Wu, R., Blaabjerg, F., Wang, H., Liserre, M. and Iannuzzo, F. (2013). Catastrophic failure and fault-tolerant design of IGBT power electronic converters – An overview. In: *IECON 2013 - 39th Annual Conference of the IEEE Industrial Electronics Society. Presented at the IECON 2013 – 39th Annual Conference of the IEEE Industrial Electronics Society*, Vienna, Austria: IEEE, pp. 507–513. doi: 10.1109/IECON.2013.6699187.

Zhang, X., Zhao, T., Mao, W., Tan, D. and Chang, L. (2018). Multilevel Inverters for Grid-Connected Photovoltaic Applications: Examining Emerging Trends. *IEEE Power Electronics Magazine*, 5, pp. 32–41. doi: 10.1109/MPEL.2018.2874509.